11th World Congress on Computational Mechanics (WCCM XI)
5th European Conference on Computational Mechanics (ECCM V)
6th European Conference on Computational Fluid Dynamics (ECFD VI)
E. Oñate, J. Oliver and A. Huerta (Eds)

FAST MULTIPOLE BOUNDARY ELEMENTS METHOD FOR MULTIZONE PROBLEMS

T. TRINH[*†], S. MOUHOUBI[†], C. CHAZALLON[†] AND M. BONNET[††]

[†] Laboratory ICUBE, UMR 7357
National Institute of Applied Sciences (INSA) of Strasbourg
24, boulevard de la Victoire, 67084, Strasbouef Cedex, France
e-mail: quoctuan.trinh@insa-strasbourg.fr, web page: http://www.insa-strasbourg.fr/

[††]Laboratory POEMS UMR 7231
Superior National School of Adavanced Techniques (ENSTA ParisTech)
1024, boulevard des Marchaux, 91762 Palaiseau Cedex
e-mail: marc.bonnet@ensta-paristech.fr - Web page: http://www.ensta-paristech.fr

Key words: SGBEM, FMM, Multizone Problems, Flexible GMRES

Abstract. Domains containing internal boundaries such as interface occur in many applications: composite materials, geophysical simulations... The treatment of these problems requires the continuity across the common boundary. There are usually more unknowns on interfaces which render the solution of a multizone problem more sophisticated and inefficient. Among many numerical alternatives, the symmetric Galerkin boundary elements (SGBEM) provides a natural treatment on the interfaces and produces a symmetric coefficient matrix of reduced size. Taking into account the distinct advantages of the BEM in treating unbounded or evolutive problems, the SGBEM is also able to study accurately fracture problems. Moreover, with help of the Fast Multipole Method (FMM), the method can surpass all the limitations of the standard boundary analysis and become a very powerful and efficient tool. In this paper, we present the implementation of the Fast Multipole Method in the SGBEM and report some examples of non-fractured and fractured multizone problems.

1 INTRODUCTION

Practical problems are usually presented with heterogeneity. The treatment of these problems leads to the study of the interface between different materials. In a generic multizone problem, there are additional unknowns due to the presence of interfaces. These unknowns belong to all adjacent bodies and are governed by the continuity condition (Eg. displacement $\mathbf{u_1} = \mathbf{u_2}$ and traction $\mathbf{t_1} = -\mathbf{t_2}$ in elastostatics). The construction of the global coefficient matrix and the resolution of the system become therefore more difficult.

The SGBEM normally provides a symmetric matrix, but when applied for a sub-domain, this property can not be completely achieved. In order to conserve the global symmetry of the method, an appropriate technique must be adopted during the matrices construction. Layton et al.[10] introduced an algorithm that can lead to a partly symmetric matrix by putting the unknowns on the interface ahead. The block matrices corresponding to interfaces are non-symmetric, while the rests are symmetric. In [6], Gray and Paulino studied a fully symmetric Galerkin BEM in heat transfer. This method is based on an appropriate combination of usual SGBEM equations on interfacial and non-interfacial boundaries. This technique is later adopted in elastostatics[4] and fracture mechanics[9]. With the advantageous nature and symmetry in treating multizone problems, the SGBEM becomes therefore a formidable option. The need of solving practical multizone issues which feature high amounts of unknowns naturally leads to the application of the Fast Multipole Method. With the complexity of $O(Nlog^{\alpha}N)$, the multizone FM-SGBEM is expected to be a powerful alternative for many important realistic applications.

In this work, the approach described in [6] by Gray and Paulino has been exploited. Perfect bonding between sub-domains is assumed first, imposing the continuity of displacement and the equilibrium of traction across the interface. Via some appropriate terms rearrangement and sign adoptions, the symmetry of the global matrix can be achieved. Secondly, the Fast Multipole Method is introduced in the multizone SGBEM formulation. Some computational and efficiency issues of the algorithm is discussed in the later subsection. Lastly, numerical experiments on validation tests are given and one extension on practical material is reported, followed by some conclusions and perspectives.

2 MATHEMATICAL BACKGROUND

2.1 Symmetric Galerkin BEM in fracture mechanics

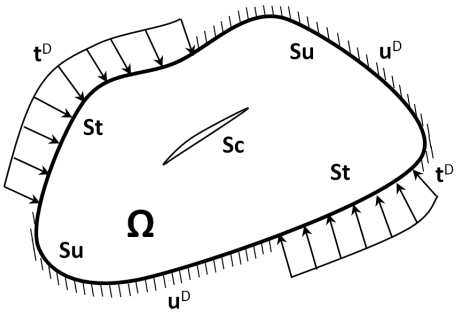

Figure 1: Solid containing a crack

Considering a fractured solid Ω subjected to prescribed tractions t^D on the boundary St and displacement constraints u^D on Su. The boundary of Ω (including the crack S_c) is thus defined as $S = S_t \bigcup S_u \bigcup S_c$. S_c is conceived as a locus of displacement discontinuity,

the jump of the displacements can be computed as $\boldsymbol{\Delta u}(x) = \boldsymbol{u}(x^+) - \boldsymbol{u}(x^-)$ where $\boldsymbol{u}(x^+)$ and $\boldsymbol{u}(x^-)$ are respectively the displacement of the upper and lower faces of the crack ($S_c = S_c^- \bigcup S_c^+$). The direction of the normal of the crack is by convention, pointing from S^- to S^+. Details of the mathematical developments of the SGBEM can be found in [5]. The boundary integral formulation for this problem is written as follow:

$$\left\{ \begin{array}{l} \mathcal{B}_{uu}(\mathbf{u}, \tilde{\mathbf{u}}) + \mathcal{B}_{tu}(\mathbf{t}, \tilde{\mathbf{u}}) + \mathcal{B}_{\Delta uu}(\boldsymbol{\Delta u}, \tilde{\mathbf{u}}) = \mathcal{F}_u(\tilde{\mathbf{u}}) \\ \mathcal{B}_{ut}(\mathbf{u}, \tilde{\mathbf{t}}) + \mathcal{B}_{tt}(\mathbf{t}, \tilde{\mathbf{t}}) + \mathcal{B}_{\Delta ut}(\boldsymbol{\Delta u}, \tilde{\mathbf{t}}) = \mathcal{F}_t(\tilde{\mathbf{t}}) \\ \mathcal{B}_{u\Delta u}(\mathbf{u}, \boldsymbol{\Delta \tilde{u}}) + \mathcal{B}_{t\Delta u}(\mathbf{t}, \boldsymbol{\Delta \tilde{u}}) + \mathcal{B}_{\Delta u\Delta u}(\boldsymbol{\Delta u}, \boldsymbol{\Delta \tilde{u}}) = \mathcal{F}_{\Delta u}(\boldsymbol{\Delta \tilde{u}}) \end{array} \right. \tag{1}$$

The explicit representations of these terms are detailed in [1], we introduce here $\mathcal{B}_{tt}$, $\mathcal{B}_{tu}$ and $\mathcal{B}_{\Delta u\Delta u}$ for example:

$$\begin{aligned} \mathcal{B}_{tt}(\mathbf{t}, \tilde{\mathbf{t}}) &= \int_{S_u}\int_{S_u} t_k(\mathbf{x}) U_i^k(\mathbf{x}, \tilde{\mathbf{x}}) \tilde{t}_i(\tilde{\mathbf{x}}) dS_{\tilde{x}} dS_x \\ \mathcal{B}_{tu}(\mathbf{t}, \tilde{\mathbf{u}}) &= -\int_{S_u}\int_{S_T} t_k(\mathbf{x}) T_i^k(\mathbf{x}, \tilde{\mathbf{x}}) \tilde{u}_i(\tilde{\mathbf{x}}) dS_{\tilde{x}} dS_x \\ \mathcal{B}_{\Delta u\Delta u}(\boldsymbol{\Delta u}, \tilde{\boldsymbol{\Delta u}}) &= \int_{S_c}\int_{S_c} [R\Delta u]_{iq}(\mathbf{x}) B_{ikqs}(\mathbf{r}) [R\Delta \tilde{u}]_{ks}(\tilde{\mathbf{x}}) dS_{\tilde{x}} dS_x \end{aligned} \tag{2}$$

$\mathbf{u}, \mathbf{t}$ and $\boldsymbol{\Delta u}$ are respectively the unknown on S_t, S_u and S_c; $U_i^k(\mathbf{x}, \tilde{\mathbf{x}})$ and $T_i^k(\mathbf{x}, \tilde{\mathbf{x}})$ are respectively the i^{th} displacement and traction of $\mathbf{x}$ due to a point load at $\tilde{\mathbf{x}}$ in the direction of the k^{th} coordinate axis. For $\mathbf{x}$ and $\tilde{\mathbf{x}} \in \mathcal{R}^3$, they are called Kelvin fundamental solutions and are written as:

$$U_i^k(\mathbf{x}, \tilde{\mathbf{x}}) = \frac{1}{16\pi\mu(1-\nu)r}[\hat{r}_i\hat{r}_k(3-4\nu) + \delta_{ik}] \tag{3}$$

$$T_i^k(\mathbf{x}, \tilde{\mathbf{x}}) = -\frac{1}{8\pi(1-\nu)r^2} n_j(\mathbf{x})[3\hat{r}_i\hat{r}_k\hat{r}_j + (1-2\nu)(\delta_{ik}\hat{r}_j + \delta_{jk}\hat{r}_i - \delta_{ij}\hat{r}_k)] \tag{4}$$

having set

$$\mathbf{r} = \mathbf{x} - \tilde{\mathbf{x}}, \qquad r = \|\mathbf{r}\|, \qquad \hat{\mathbf{r}} = \mathbf{r}/r \tag{5}$$

The surface curl operator R is defined as:

$$[Ru]_{ks}(\tilde{\mathbf{x}}) = e_{jfs} n_j u_{k,f}(\tilde{\mathbf{x}}) \tag{6}$$

while the weakly singular fourth-order tensor B_{ikqs} is given by:

$$B_{ikqs}(\mathbf{r}) = \frac{1}{8\pi(1-\nu)r}[2\delta_{qs}\hat{r}_i\hat{r}_k + 2(\delta_{ik}\delta_{qs} - 2\nu\delta_{is}\delta_{kq} - (1-\nu)\delta_{iq}\delta_{ks})] \tag{7}$$

Weak continuity requirements ($C^{0,\alpha}$) are enforced on $\mathbf{u}, \boldsymbol{\Delta u}, \tilde{\mathbf{u}}, \boldsymbol{\Delta \tilde{u}}$ which is less restrictive than the collocation approach ($C^{1,\alpha}$). The SGBEM can therefore deal with hypersingular

and other singular integral boundary equations only by means of standard continuous elements. Besides, the discretized matrix is symmetric. These features make SGBEM numerically superior to the collocation approach. Still, the limit of the method is the fact that the double integrals typically give rise to a fully-populated matrix. Some practical issues (which normally have a number of unknowns $> 10^5$) could not be solved by SGBEM due to the excessive amount of operation counts and of memory requirements.

2.2 Multizone SGBEM

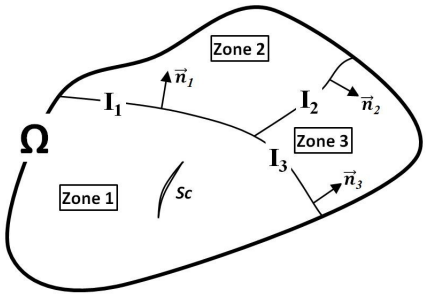

Figure 2: A multizone fractured domain

Considering a fractured solid Ω containing 3 homogeneous sub-domains (Fig. 2). On an interface, both displacements and tractions are unknowns. The continuity of displacement and equilibrium condition are: $\mathbf{u}^a(\mathbf{x}) = \mathbf{u}^b(\mathbf{x})$ and $\mathbf{t}^a(\mathbf{x}) = -\mathbf{t}^b(\mathbf{x})$ knowing that a, b represent two adjacent zones. Let us consider a generic sub-domain (body) i sharing n interfaces with its surrounding zones, the formulation of SGBEM can be written as:

$$[K]^i\{x\}^i = \{b\}^i \tag{8}$$

$[K]^i$, $\{x\}^i$ and $\{b\}^i$ are respectively the coefficient matrix, solution vector and local known vector corresponding to $body - i$. While $\{x\}^i = (u^{S_t}, t^{S_u}, \Delta u^{S_c}, u^{I_1}, t^{I_1}, ..., u^{I_n}, t^{I_n})^T$ contains the global unknowns related to this body, $[K]^i$ stores all the local coefficients and takes the following form:

$$\begin{bmatrix}
B_{uu}^{S_tS_t} & B_{tu}^{S_uS_t} & B_{\Delta uu}^{S_cS_t} & B_{uu}^{I_1S_t} & \circ B_{tu}^{I_1S_t} & ... & B_{uu}^{I_nS_t} & \bullet B_{tu}^{I_nS_t} \\
B_{ut}^{S_tS_u} & B_{tt}^{S_tS_t} & B_{\Delta ut}^{S_cS_t} & B_{ut}^{I_1S_u} & \circ B_{tt}^{I_1S_u} & ... & B_{ut}^{I_nS_u} & \bullet B_{tt}^{I_nS_u} \\
B_{u\Delta u}^{S_tS_c} & B_{t\Delta u}^{S_uS_c} & B_{\Delta u\Delta u}^{S_cS_c} & B_{u\Delta u}^{I_1S_c} & \circ B_{t\Delta u}^{I_1S_c} & ... & B_{u\Delta u}^{I_nS_c} & \bullet B_{t\Delta u}^{Si_nS_c} \\
B_{uu}^{S_tI_1} & B_{tu}^{S_uI_1} & B_{\Delta uu}^{S_cI_1} & B_{uu}^{I_1I_1} & \circ(B_{tu}^{I_1I_1} + I_u^1) & ... & B_{uu}^{I_nI_1} & \bullet B_{tu}^{I_nI_1} \\
\circ B_{ut}^{S_tI_1} & \circ B_{tt}^{S_uI_1} & \circ B_{\Delta ut}^{S_cI_1} & \circ(B_{ut}^{I_1I_1} - I_t^1) & B_{tt}^{I_1I_1} & ... & B_{ut}^{I_nI_1} & \circ \bullet B_{tt}^{I_nI_1} \\
... & ... & ... & ... & ... & ... & ... & ... \\
B_{uu}^{S_tI_n} & B_{tu}^{S_uI_n} & B_{\Delta uu}^{S_cI_n} & B_{uu}^{I_1I_n} & B_{tu}^{I_1I_n} & ... & B_{uu}^{I_nI_n} & \bullet(B_{tu}^{I_nI_n} + I_u^n) \\
\bullet B_{ut}^{S_tI_n} & \bullet B_{tt}^{S_uI_n} & \bullet B_{\Delta ut}^{S_cI_n} & \bullet B_{ut}^{I_1I_n} & \bullet \circ B_{tt}^{I_1I_n} & ... & \bullet(B_{ut}^{I_nI_n} - I_t^n) & B_{tt}^{I_nI_n}
\end{bmatrix} \tag{9}$$

$[B_{**}]$ and $[I_*]$ denote double and single integrals in SGBEM formulation (details in [1]). The subscripts show the integral types and the superscripts denote the surfaces on which the integral equations are written. We notice that the single integral $[I_u^{S_i}]$ is in general, different with the transpose of $[I_t^{S_i}]$ which renders the local coefficient matrix of this zone non-symmetric. Fortunately, during assembly process, these terms are all canceled because of the equivalent terms from another zone which are equal but of opposite-signs. This eventually results in a global symmetric matrix. Symbols $\circ$ or $\bullet$ indicate where correct signs for interfacial tractions are accounted for (see [4]).

2.3 Fast Multipole Method

The Fast multipole method (by Rohklin [8] and Greengard) is an alternative technique to enhance the performance of a boundary integral analysis. The FMM can be illustrated in Fig.3a: to compute a double integral between $\boldsymbol{S_x}$ and $\boldsymbol{S_y}$, all the contributions from $\boldsymbol{S_y}$ are first shifted to an intermediate pole O then transferred eventually to every evaluation point in $\boldsymbol{S_x}$. Without having to repeat the usual double surface integral, the FMM requires thus only $m + n$ instead of $m.n$ operations. This operations saving becomes significant especially in the iterative resolution of a boundary analysis. With no need to construct a coefficient matrix and the complexity cut down to $O(Nlog^{\alpha}N)$, the FM-SGBEM becomes very efficient in treating large-scale analysis. In SGBEM, the FMM reformulates the

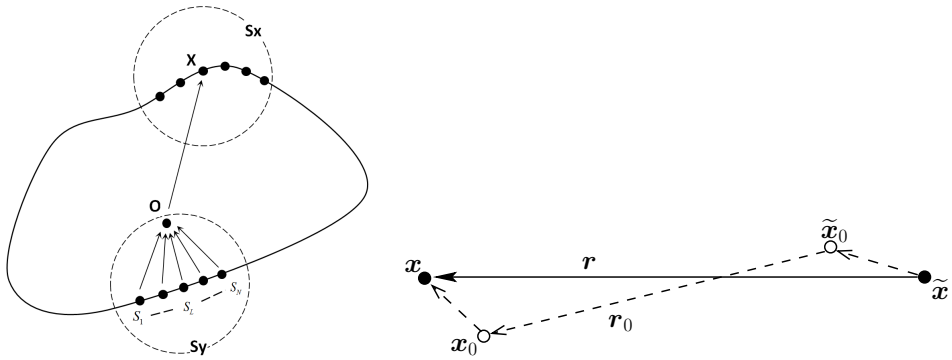

Figure 3: (a) Simple illustration of the Fast Multipole algorithm (b) Decomposition of the position vector : notation

kernels U_i^k, T_i^k, B_{ikqs} into multipole series, which achieves a complete separation of the variables $\mathbf{x}$ and $\tilde{\mathbf{x}}$. For this purpose, the relative solution vector $\mathbf{r} = \mathbf{x} - \tilde{\mathbf{x}}$ (see Fig.3b) is decomposed into $\mathbf{r} = \mathbf{x'} + \mathbf{r}_0 - \tilde{\mathbf{x}}'$ with $\mathbf{r}_0 = \mathbf{x}_0 - \tilde{\mathbf{x}}_0$, $\mathbf{x'} = \mathbf{x} - \mathbf{x}_0$ and $\tilde{\mathbf{x}}' = \tilde{\mathbf{x}} - \tilde{\mathbf{x}}_0$ in terms of 2 poles $\mathbf{x}_0, \tilde{\mathbf{x}}_0$. With these notations, the multipole expansion of $1/r$ (read [3]) is

given by:

$$\frac{1}{r} = \sum_{n=0}^{\infty} \sum_{m=-n}^{n} (-1)^n R_{nm}(\tilde{\mathbf{x}}') \sum_{n'=0}^{n} \sum_{m'=-n'}^{n'} \overline{S_{n+n',m+m'}(\mathbf{r}_0)} R_{n'm'}(\mathbf{x}') \tag{10}$$

$$R_{nm}(\mathbf{y}) = \frac{1}{(n+m)!} P_n^m(cos\alpha) e^{im\beta} \rho^n$$

$$S_{nm}(\mathbf{y}) = (n-m)! P_n^m(cos\alpha) e^{im\beta} \frac{1}{\rho^{n+1}}$$

(ρ, α, β) being the spherical coordinates of the argument $\mathbf{y}$ and P_n^m denoting the Legendre polynomials, and with the overbar denoting complex conjugation. For given poles $\mathbf{x}_0, \tilde{\mathbf{x}}_0$, the above expansion (10) is convergent for any $\mathbf{x}_0, \tilde{\mathbf{x}}_0$ such that:

$$\|\mathbf{x}'\| < \|\tilde{\mathbf{x}}' - \mathbf{r}_0\| \qquad and \qquad \|\tilde{\mathbf{x}}'\| < \|\mathbf{x}' + \mathbf{r}_0\| \tag{11}$$

Let $\Gamma(\mathbf{x}_0)$ and $\tilde{\Gamma}(\tilde{\mathbf{x}}_0) \subset \partial\Omega$ denote two subsets of $\partial\Omega$ such that 10 hold for any $\mathbf{x} \in \Gamma(\mathbf{x}_0)$ and $\tilde{\mathbf{x}} \in \tilde{\Gamma}(\tilde{\mathbf{x}}_0)$. Then the contribution of surfaces $\Gamma(\mathbf{x}_0), \tilde{\Gamma}(\tilde{\mathbf{x}}_0)$ to the bilinear form $\mathcal{B}_{tt}(\mathbf{t}, \tilde{\mathbf{t}})$, denoted by $\mathcal{B}_{tt}(\mathbf{x}_0, \tilde{\mathbf{x}}_0)$, is given by:

$$\mathcal{B}_{tt}(\mathbf{x}_0, \tilde{\mathbf{x}}_0) = \int_{\Gamma(\mathbf{x}_0)} \int_{\tilde{\Gamma}(\tilde{\mathbf{x}}_0)} t_k(\mathbf{x}) U_i^k(\mathbf{x}, \tilde{\mathbf{x}}) \tilde{t}_i(\tilde{\mathbf{x}}) dS_{\tilde{x}} dS_x \tag{12}$$

and can be evaluated by replacing the kernel U_i^k by its multipole expansion, and likewise for the other bilinear forms. For simplicity, only the contribution $\mathcal{B}_{tt}(\mathbf{x}_0, \tilde{\mathbf{x}}_0)$ is detailed here. The treatment of the other bilinear forms follow the same approach. By substituting (10) into (12), the contribution $\mathcal{B}_{tt}(\mathbf{x}_0, \tilde{\mathbf{x}}_0)$ can be written as:

$$\mathcal{B}_{tt}(\mathbf{x}_0, \tilde{\mathbf{x}}_0) = \sum_{n=0}^{\infty} \sum_{m=-n}^{n} (-1)^n \sum_{n'=0}^{\infty} \sum_{m'=-n'}^{n'} \Big\{ \tilde{M}^1_{knm}(\tilde{\mathbf{x}}_0) \overline{S_{n+n',m+m'}(\mathbf{r}_0)} M^1_{kn'm'}(\mathbf{x}_0) +$$
$$\tilde{M}^1_{knm}(\tilde{\mathbf{x}}_0) r_{0k} \overline{S_{n+n',m+m'}(\mathbf{r}_0)} M^2_{n'm'}(\mathbf{x}_0) + \tilde{M}^2_{nm}(\tilde{\mathbf{x}}_0) \overline{S_{n+n',m+m'}(\mathbf{r}_0)} M^2_{n'm'}(\mathbf{x}_0) \Big\} \tag{13}$$

In terms of the multipole moments

$$M^1_{knm}(\mathbf{x}_0) = \int_{S_u} R_{nm}(\mathbf{x}') t_k(\mathbf{x}') dS'_x$$
$$M^2_{nm}(\mathbf{x}_0) = \int_{S_u} R_{nm}(\mathbf{x}') x'_k t_k(\mathbf{x}') dS'_x \tag{14}$$

associated to the pole $\mathbf{x}_0$ and

$$\tilde{M}^1_{knm}(\tilde{\mathbf{x}}_0) = \int_{S_u} [\delta_{ik} - (3-4\nu)\tilde{x}_k \frac{\partial}{\partial \tilde{x}_i}] R_{nm}(\tilde{\mathbf{x}}') \tilde{t}_i(\tilde{\mathbf{x}}') dS'_x$$
$$\tilde{M}^2_{nm}(\tilde{\mathbf{x}}_0) = (3-4\nu) \int_{S_u} \frac{\partial}{\partial \tilde{x}_i} R_{nm}(\tilde{\mathbf{x}}') \tilde{t}_i(\tilde{\mathbf{x}}') dS'_x \tag{15}$$

associated to the pole $\tilde{\mathbf{x}}_0$. Equation 13 can be recast into the following equivalent form

$$\mathcal{B}_{tt}(\mathbf{t},\tilde{\mathbf{t}}) = \sum_{n=0}^{\infty}\sum_{m=-n}^{n}(-1)^n\Big\{\tilde{M}^1_{knm}(\tilde{\mathbf{x}}_0)L^1_{knm}(\tilde{\mathbf{x}}_0) + \tilde{M}^2_{nm}(\tilde{\mathbf{x}}_0)L^2_{nm}(\tilde{\mathbf{x}}_0)\Big\} \tag{16}$$

in terms of the local expansion coefficients, related to the multipole moments by the following multipole-to-local (M2L) relation:

$$\begin{aligned} L^1_{knm}(\mathbf{x}_0) &= \sum_{n'=0}^{n}\sum_{m'=-n'}^{n'}\overline{S_{n+n',m+m'}(\mathbf{r}_0)}[M^1_{kn'm'}(\mathbf{x}_0) + r_{0k}M^2_{n'm'}(\mathbf{x}_0)] \\ L^2_{nm}(\mathbf{x}_0) &= \sum_{n'=0}^{n}\sum_{m'=-n'}^{n'}\overline{S_{n+n',m+m'}(\mathbf{r}_0)}M^2_{n'm'}(\mathbf{x}_0) \end{aligned} \tag{17}$$

3 NUMERICAL IMPLEMENTATION

Algorithm 1 Multizone FM-SGBEM

(a) Import Geometries, Parameters + Build *octree*
(b) Compute known terms
- **Do** i = 1,nbody *(Loop on all bodies)*
  Call <upward>$_i$ → <downward>$_i$ → <expansion>$_i$
  → compute $\{b\}_i$ → $\{b\}_{global} := \{b\}_{global} + \{b\}_i$
  → compute and store $[Knears]_{zone\ i}$
- **EndDo**

(c) Iterative Solution
Outer GMRES (precision 10^{-3})
- Global Matrix-Vector multiplication
  - **Do** i = 1,nbody *(Loop on all bodies)*
    Call <upward>$_i$ → <downward>$_i$ → <expansion>$_i$
    → compute $[K]_{zone\ i}\{x\}_i = [Knears]_{zone\ i}\{x\}_i + [K^{FMM}]_{zone\ i}\{x\}_i$
    → store the product $[K]\{x\} := [K]\{x\} + [K]_{zone\ i}\{x\}_i$
  - **EndDo**
- Preconditioning Task Inner GMRES (precision 10^{-1})
  - **Do** i = 1,nbody *(Loop on all bodies)*
    → compute $[Knears]\{w\} := [Knears]\{w\} + [Knears]_{zone\ i}\{w\}_i$
    → inner preconditioning
  - **EndDo**

(d) Post-Processing

Provided that each sub-domain cannot be solved separately, the multizone FM-SGBEM algorithm sets a loop on all bodies. On each body, the local values are computed and are transferred to the global arrays. By combining all the local quantities ($\{vect\_y\}_i$, $[Knear]_i$, $\{product\}_i$... i being the sub-domain name), we gain access to the global system which is well-posed and solvable. To this point, the resolution and post-processing do not differ from the mono-domain case. The details of the multizone FM-SGBEM can be expressed in the Algorithm 1.

4 NUMERICAL EXPERIMENTS

4.1 Spherical Envelope under internal pressure

The first numerical test consists of a spherical homogeneous envelope, of internal radius a and external radius b. The constitutive material is elastic isotropic ($E = 1, \nu = 0.3$). The internal surface is subjected to a normal uniform pressure $p = 1$ (see Fig.4a):

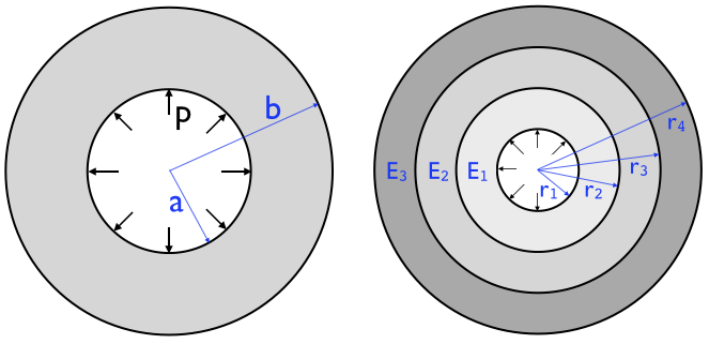

(a) (b)

Figure 4: (a) Generic spherical homogeneous envelope under internal uniform pressure (b) 3-layer spherical envelope under internal uniform pressure: $r_1 = 1, r_2 = 2, r_3 = 3, r_4 = 4$, materials: $E_1 = E_2 = E_3 = 1, \nu_1 = \nu_2 = \nu_3 = 0.3$

For this simple test, the exact solution of radial displacement u_r is:

$$u_r = \frac{a^3}{b^3 - a^3}\left[(1-2\nu)r + (1+\nu)\frac{b^3}{2r^2}\right]\frac{p}{E} \tag{18}$$

A spherical envelope composed of 3 layers has been considered. To take advantage of the exact solution, we choose identical material properties for all 3 layers. The geometry and boundary conditions can be found on Fig.4b. In this example, 518 Q8 elements have been used, constituting 13.689 unknowns (9.447 in displacements and 4.242 in traction). The FM-SGBEM program converges after 25 iterations to reach the precision of 10^{-3} (about 30' calculation). The mean values $\overline{u}_r$ are computed from the radial displacement of all nodes on different radius. The relative error between the numerical code and the exact solution are reported in the table 1 and in Fig.5. Despite the coarseness of the chosen mesh, the numerical results yield a very good agreement with the references.

4.2 Matrix-Inclusion Material

In this section, we discuss about the extension of the method into the matrix-inclusion materials (as known as composites - Fig.6). Composite materials have proven to be the subject of great interest as these materials possess better characteristics than the original components. The literature concerning the fracture of composite materials is rather

Table 1: Displacement u_r on different layers

position	u_r theorical	$\overline{u}_r$ numerical	relative error (%)
r_1	0.66667	0.6632	0.52 %
r_2	0.17778	0.176338	0.81 %
r_3	0.092416	0.0916	0.86 %
r_4	0.06667	0.0661	0.83 %

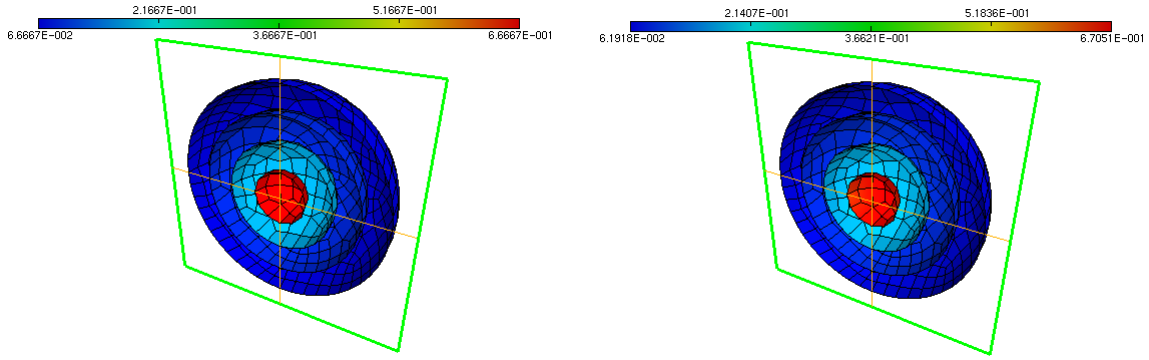

(a) (b)

Figure 5: Radial displacement of a internal-pressurized spherical envelope (a) exact results (b) numerical results

limited and restricted to extremely idealized models ([11]-[12]). In certain scales and circumstances, the response of the system should not be approximated by the macroscopic parameters. To provide a better analysis on a fractured composite material, one should take the heterogeneity of the sub-domains into consideration. Exhaustive studies on the fracture composite by different numerical approaches can be found in ([13]-[14]). In the present paper, we use the Fast Multipole-SGBEM to simply investigate the behavior of fractures (the crack opening displacement/stress intensity factors) in a model of composite.

Considering a simple configuration of a composite material (Fig.7): the outer geometry is a clamped cube of size a under uniaxial vertical tensile load $p = 1$, contains a system of n_i^3 spherical inclusions of radius r_i. These inclusions are located regularly on a cubic grid of step d_i. The solid also has a system of n_c^3 cracks inside. These cracks are oriented randomly in space and are distributed on a regular cubic grid of step d_c. To ensure a good variety for this problem, different sizes, shapes and material properties are also applied for the cracks and inclusions: Two type of cracks are considered: penny-shaped crack of radius r_c and elliptical cracks of major semi-axis a_c and minor semi-axis b_c; a scaling coefficient ranged randomly from 0.5 to 1 is applied to each crack and inclusion to vary

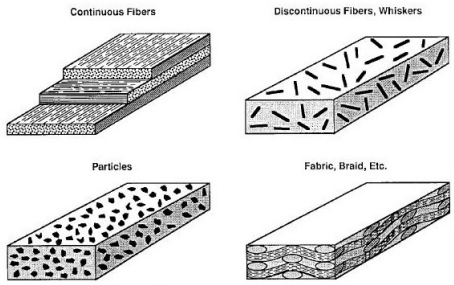

Figure 6: Composite materials

the size of these entities. While the material of solid is fixed as $E_{solid} = 1, \nu_{solid} = 0,3$, these values on inclusions are varied: $E_{inclusion} = 1 - 10$, $\nu_{inclusion} = 0,1 - 0,4$.

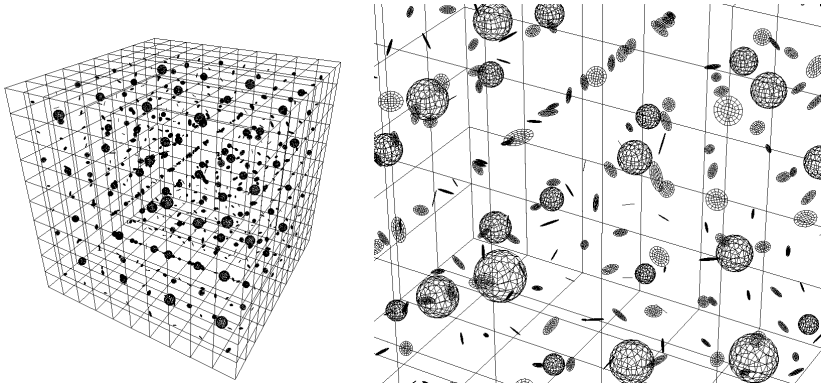

(a) (b)

Figure 7: (a) Model of fractured composite material (4x4x4 spherical inclusions & 8x8x8 cracks) (b) Interior view of cracks and inclusions

The computations consist of large-scale simulations where important numbers of inclusions and cracks are considered. The dimensions are chosen such that: $a = 80$ for the cube; for the system of cracks: $r_c = 1$, $a_c = 1$, $b_c = 0.5$; for the inclusions: $r_i = 2$, $n_i = 4$, $d_i = 20$. The outer boundary and inclusion are made of 600 and 151 Q4 elements respectively. The crack is meshed with 48 Q8 elements. The table below shows the details of the number of components in the solid as well as the number of unknowns and the output results:

The dependence of the computational time per iteration is captured and shown in Fig.8.

Table 2: Fractured composite numerical tests by Flexible FM-SGBEM: *NEQ* denotes the problem size, N-iter is the iteration counts; Pre_time, Tot_time are respectively the preparation times and total computational times.

Mesh	n_c	d_c	*NEQ*	*max_elem*	$\bar{l}$	Pre_Time(s)	N-Iter	CPU(s)/iter	Tot_Time(s)
1	8	10	258.702	30	5	7.067	17	809	21.673
2	10	7	447.558	30	8	8.890	15	1.261	29.211
3	12	6	729.294	30	8	48.121	16	2.375	88.188
4	14	5	1.122.468	30	6	31.368	14	4.404	99.623

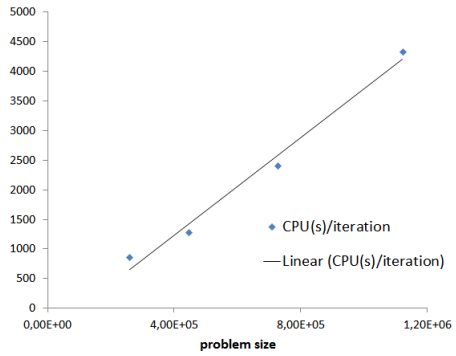

Figure 8: Time (s) consumed per iteration

5 CONCLUSIONS

In the present work, the optimized algorithm of the FM-SGBEM has been implemented in the context of multizone problems and the obtained results are of excellent accuracy. The research has also shown that the FM-SGBEM is able to deal with large-scale multizone, multifractured problems on moderate computational resources. However, realistic geometries (Eg. presence of corners/edges which share multiple sub-domains) are still very difficult to be correctly and efficiently modeled. Future developments are expected to investigate more sophisticated configurations concerning cracks inside, outside, penetrating or lying along the interface (inclusion). Practical models (Eg. Multi-layer road structures) also hold a great interest in our study. Furthermore, the authors aim to apply this method to study more interesting configurations where the crack propagation is taken into consideration.

Acknowledgements This work is funded by the European Initiative Commission INTERREG IV - Upper Rhin Program (Project B20 TEM3)

REFERENCES

[1] Pham D., Mouhoubi S., Bonnet M., Chazallon C., Fast multipole method applied to Symmetric Galerkin boundary element method for 3D elasticity and fracture problems. Eng. Anal. Bound. Elem. 2012.

[2] Chaillat S., Methode multipole rapide pour les equations integrales de frontieres en elastodynamique 3D. Application a la propagation d'ondes sismiques. Phd thesis 2008.

[3] Yoshida. K.I, Application of fast multipole to boundary integral equation method. Phd thesis 2001.

[4] Margonari M., Boundary element techniques for three dimensional problems in Elastostatics. Phd thesis 2004.

[5] Bonnet M., Boundary integral equation method for Solid and Fluids, Wiley 1999.

[6] Gray L. J., Glaucio H. Paulino, Symmetric Galerkin Boundary Integral Formulation for Interface and Multi-zone problems. Int. J. Numer. Meth. Engng., vol. 40:pp. 3085-3101, 1997.

[7] Frangi A., Novati G., Springhetti R., Rovizzi M., 3D fracture analysis by symmetric Galerkin BEM. Compt. Mech. 28 (2002) p.220-232.

[8] Rohklin V., Rapid solution of integral equations of classical potential theory. J. Comp. Phys., 60:187-207, 1985.

[9] Chen T., A symmetric Galerkin multi-zone boundary element method for cohesive crack growth. Engineering Fracture Mechanics, Vol.63, p.591-609, 1999.

[10] Ganguly S., Layton J.G., A fully symmetric multi-zone Galerkin boundary element method. Int. J. Meth. Num. Engng., Vol.44, p.991-1009, 1999.

[11] Tamate O., The effect of a circular inclusion on the stresses around a line crack in a sheet under tension. Int. J. Fract. 1968;4:257-65.

[12] Hwu C., Liang YK., Yen WJ., Interactions between inclusions and various types of cracks. Int. J . Fract. 1995;73:301-23.

[13] Li R., Chudnovsky A., A variation of the energy release rate as a crack approaches and passes through an elastic inclusion. Int. J. Fract. 1993; 59:R69-74.

[14] Wang C., Libardi W., Baldo JB., Analysis of crack extension paths and toughening in a two phase brittle particulate composite by the boundary element method. Int.J.Fract. 1998,94:177-88.